NOVA
SCIENCE PUBLISHERS, INC.

HYDRODYNAMIC COMPARISON BETWEEN SOIL UNDER BARLEY AND GRASSLAND

A. Alaoui
B. Goetz
E. Diserens

400 Oser Avenue, Suite 1600
Hauppauge, N. Y. 11788-3619
Phone (631) 231-7269
Fax (631) 231-8175
E-mail: Main@novapublishers.com
http://www.novapublishers.com

In: "Barley: Production, Cultivation and Uses"
Editor: 978-1-61209-745-9
ISBN: 978-1-61209-745-9 2012

In: Barley: Production, Cultivation and Uses
Editor: Steven B. Elfson
ISBN: 978-1-61209-745-9

Chapter 9

HYDRODYNAMIC COMPARISON BETWEEN SOIL UNDER BARLEY AND GRASSLAND

***A. Alaoui*[1*], *B. Goetz*[1] *and E. Diserens*[2]**
[1]Hydrology Group, Department of Geography, University of Bern, Hallerstrasse 12, CH–3012 Bern, Switzerland
[2]Research Station Agroscope Reckenholz-Tänikon ART, CH–8356 Ettenhausen, Switzerland

ABSTRACT

The main aim of this study was to verify the hydrodynamic aspects identified by the 1D (vertical) information obtained by the MACRO model with the 2D image analysis of the blue patches in two different soils: site 1 used as grassland and site 2 for growing barley. In addition, the impact of the land use (compaction and tillage) was assessed in the two sites. Water exchange rate (WER) from macropores into the surrounding soil matrix was investigated to determine the efficiency of macropores in conducting water in both sites. The MACRO model successfully reproduced the patterns of the soil moisture measurements under non-equilibrium conditions for the grassland and barley sites. Due to the small matrix conductivities of such fine textures, the linings of macropores strongly limit mass exchange in the two sites. As a result, WER was very low in view of the high input intensity. The fact that the highest dye tracer concentration values are found in the topsoil of the grassland site, together with the lowest values of simulated WER, shows that the more tortuous macropores have been destroyed by compaction. Consequently, only the larger, less tortuous macropores remain and are efficient. In barley site, there was a higher pore volume with a diameter larger than 50 μm compared to grassland soil for same soil horizons. While, in the topsoil of barley site, the loosening effect may be due to the tillage, in the subsoil, this fact maybe attributed to the root system of the barley. The loosening effect of tillage in the topsoil of the barley site revealed in the laboratory analysis is confirmed by the results of MACRO simulations (small values of *n**, reflecting pore size distribution and tortuosity and WER).

[*] Corresponding author. Tel. +41-31-6318557; fax: +41-31-6318511. E-mail: alaoui@giub.unibe.ch

Keywords: barley; grassland; soil structure; land use; water exchange rate; dye pattern.

1. INTRODUCTION

During preferential flow, local wetting-fronts may penetrate to considerable depths in a soil profile, essentially bypassing the matrix pore space (e.g., Jarvis, 2007; Köhne et al., 2009a; 2009b). Preferential flow is characterized by highly variable patterns of water percolation. Occurring of preferential flow does not imply the fully saturation of entire soil profile (Jarvis, 2007). Near saturation of soil surface is sufficient to promote preferential flow.

Macropore flow is a subset of preferential flow that occurs in continuous root channels, earthworm burrows, fissures, or cracks in structured soil (e.g., Hendrickx and Flury, 2001). Its initiation during infiltration depends on the initial matrix water content, intensity and amount of rainfall, matrix conductivity, and soil surface contributing area (e.g., Jarvis, 2007; Köhne et al., 2009a, 2009b).

Despite the large demand for experiments to explore the causes and extent of macropore flow initiation (Flühler et al., 1996), quantitative descriptions of flow in macroporous soils under field situations are still rather limited to a few studies (e.g., Othmer et al., 1991, Bronswijk et al., 1995; Ritsema and Dekker, 1995) or restricted to relatively simplified systems or boundary conditions.

Even though profile-scale dye tracing studies in soils have provided further convincing visual evidence of the importance control of horizon morphology and structure on preferential flow, modelling is indispensable in assessing the hydrodynamic aspect of the flow process as such. Accordingly, Jarvis (1994) developed a physically-based model (MACRO) of water and solute transport in macroporous soil. The model may be run in either one or two flow domains, allowing quantitative evaluation of preferential flow and solute transport in field soils. Water exchange rate (WER), which is predicted by the model, is of great importance for describing water flow in macroporous soils, because it largely determines the impact of macropores on the overall infiltration process at the plot scale. Lateral mass exchange between macropores and surrounding matrix is also one of the critical processes describing water flow in macroporous soils (Logsdon et al., 1996; Faeh et al., 1997).

Despite the enormous progress that has been made to demonstrate in a more quantitative manner the clear links between the texture and morphology of soil horizons using images analysis (Kulli et al., 2003; Alaoui and Helbling, 2006), no attempt was made to link between qualitative analysis of dye tracer and the hydrodynamic aspect of flow, since dye tracer experiments are related to specific soil conditions. In fact, a comparison of the experimental results is therefore rather difficult. To directly compare the flow patterns in different soils of different vegetations, it is necessary to use same experimental conditions.

Experimental evidence shows that agricultural soils are subject to loosening process by tillage and load bearing processes by traffic during the seasonal production cycle. As a result of different natural and man-induced changes in soil structure and strength, trafficability, in turn, follows a dynamic pattern during a year.

The main aim of this study is to compare between the barley and the grassland soils using 1D (vertical) information obtained by the MACRO model and the 2D image analysis of the resultant blue patches supplemented with soil textural data and pore size distribution.

2. MATERIAL AND METHODS

2.1. Location and Soil Description

The data used in this paper were taken from Alaoui and Goetz (2008). The experimental area is located near Oensingen in the Canton of Soleure, Switzerland (Swisstopo coordinates: 622 350/237 390). The area is situated in the Swiss Central Plateau (450 m a.s.l.), and the soil of the two sites has developed on clayey alluvial deposits down to a depth of about 1.6 m. The soil has been classified as Eutric-Stagnic Cambisol. Its texture consists of silty clay to a depth of 0.70 m (Table 1). Its organic carbon content varies from topsoil (2.8 %) to subsoil (0 %). A pH of 5.5 was measured near the soil surface; the value gradually increased to 5.9 at a depth of 0.60 m. The porosities range between 0.44 and 0.49 m^3 m^{-3}. Because of the high clay content (43–52 %) the soil also has moisture expansion properties, which causes cracks when the material is dry. Below the B1 horizon, the water table varies between −1 and −2 m, but may drop below −4 m during extreme dry periods, such as in summer 2003. A network of macropores comprising root and earthworm channels was visible to a depth of 0.70 m. Textural analysis and measurements of organic matter and pH were performed for site 1.

On 3rd August 2004 winter wheat was harvested with a combine harvester, and eleven days later the soil was loosened to a depth of 0.1 m using a chisel plough; shortly afterwards winter barley was sowed, which was harvested with two combine harvesters on 14th July 2005. A week later stubble and soil treatment was conducted to a depth of 0.2–0.3 m by using a chisel plough. Three successive water irrigations were applied in both sites on 11th July and 8th August 2005 respectively. On 23rd August 2005, a dye infiltration experiment was carried out in site 1. The methods of basic soil parameters analysis were described in Alaoui and Goetz (2008).

A field track separates the grassland and barley sites (Figure 1). Site 1 is nearer to this track, which is occasionally used by farmers with heavy machines. This may account for the relative compaction of its soil surface. In site 1 the sections were excavated parallel to the field track. Section 0 m was closest to the field track while section 1 m was furthest away. Consequently, we expected soil compaction to decrease from section 0 m to section 1 m.

Table 1. Basic soil properties in Oensingen (grassland - site 1)

Depth Interval (m)	Particle size distribution (%)			Texture	Organic matter OM (%)	pH
	Clay (< 2 µm)	Silt (2–60 µm)	Sand (> 60 µm)			
0–0.25	43.0	47.5	9.5	Silt clay	2.8	5.5
0.25–0.40	45.2	46.3	8.5	Silt clay	1.3	5.9
0.40–0.60	47.6	45.9	6.5	Silt clay	0.6	5.9
0.60–0.70	52.4	41.6	6.0	Silt clay	0	5.9

Texture, organic matter OM and pH of site 1. Textural classification was according to the USDA soil taxonomy.

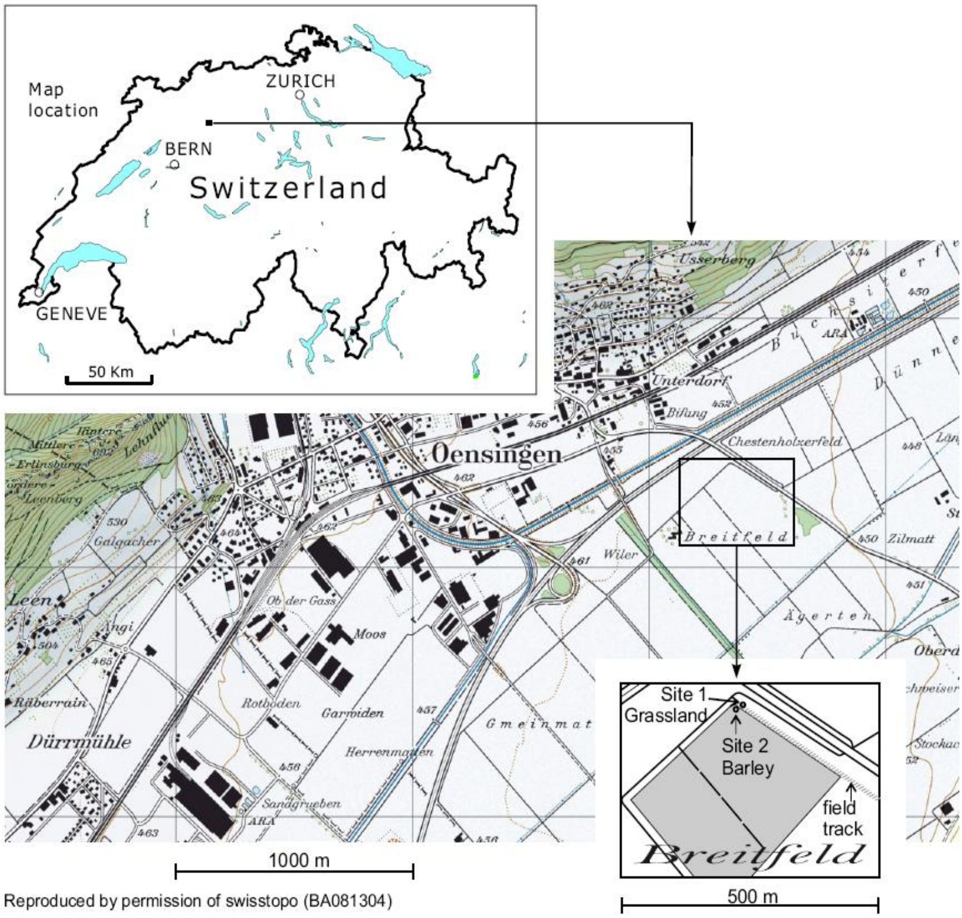

Figure 1. Location of the experimental area, region Oensingen, Canton of Soleure, Switzerland.

2.2. Water Infiltration Experiments

Three Time Domain Reflectrometry (TDR) probes were inserted diagonally from the soil surface to three depth ranges (0.20–0.30 m, 0.30–0.40 m and 0.60–0.70 m) in site 1 and two depth ranges (0.30–0.40 m and 0.60–0.70 m) in site 2. In order to take different soil moisture levels into consideration, three successive irrigations were conducted in either site. The duration of each irrigation was 1.5 hours and the intensity was 30 mm h^{-1}. No ponding was observed. Soil moisture θ was measured using TDR (TDR100 cable tester), with 0.20 m wave guides (two parallel rods of 6 mm diameter). The calibration was performed according to Roth et al. (1990). The precision of the θ measurements was assessed when flow had ceased, i.e. when a linear regression of $\theta(t)$ no longer showed a significant temporal trend. The standard errors $s_{\bar{\theta}}$ of various sets of 30 soil moisture readings, collected during this study and previous ones, never exceeded 0.015 m^3 m^{-3}. The instrument noise was thus set at $d\theta = 0.02$ m^3 m^{-3}, and any variation in water content – measured using wave guides – that exceeded $\pm d\theta$ was considered significant. Irrigation was supplied by a rainfall simulator: a metallic disc with a surface of 1 m^2 which is perforated with 100 holes attached to small tubes that lead into a reservoir. The metallic disc is moved by an electric motor, and the irrigation intensity is controlled by a flow meter. The irrigation experiments were carried out during days without precipitation.

2.3. MACRO Model

The MACRO model is a mechanistic dual-porosity model of water movement and solute transport in macroporous soils. The model is briefly introduced in this section since it was described in details in Jarvis (1994). The model divides the total soil porosity into macropores and micropores. Water flow in micropores is calculated using the Richards' (1931) equation, while macropore flow is simulated as a power law function of macropore saturation. Net rainfall is partitioned into an amount taken up by micropores and an excess amount of water flowing into macropores under non-equilibrium conditions, thereby bypassing the matrix. Water flow in the macropores is calculated with an approach derived from Darcy's law assuming a unit hydraulic gradient and simple power law function to represent the unsaturated hydraulic conductivity:

$$q_{ma} = \left(K_s - K_b\right)\left(\frac{\theta_{ma}}{\theta_s - \theta_b}\right)^{n^*} \tag{1}$$

where the subscript 'ma' refers to macropores, θ_{ma} (m^3 m^{-3}) is the macropore water content, θ_s (m^3 m^{-3}) is the saturated water content, θ_b (m^3 m^{-3}) is the boundary water content, K_s (m s^{-1}) is the saturated hydraulic conductivity, K_b (m s^{-1}) is the boundary hydraulic conductivity and n^* (-) reflects pore size distribution and tortuosity in the macropore system.

The rate of lateral water exchange from macropores to micropores S_w (s^{-1}) is treated as a first-order approximation to a diffusion-type process (Booltink et al., 1993). Assuming that gravity has negligible influence, S_w is given by (2):

$$S_w = \left[\frac{3D_w\gamma_w}{d^2}\right]\left(\theta_b - \theta_{mi}\right) \tag{2}$$

where D_w (m^2 s^{-1}) is an effective water diffusivity, γ_w (-) is a scaling factor, d (mm) is an effective diffusion pathlength which controls the mass exchange between the domains, θ_{mi} (m^3 m^{-3}) is the current water content of micropores (Jarvis, 1994). The effective water diffusivity is assumed to be given by (3):

$$D_w = \left(\frac{D_{\theta b} + D_{\theta mi}}{2}\right)S_{ma} \tag{3}$$

where $D_{\theta b}$ (m^2 s^{-1}) and $D_{\theta mi}$ (m^2 s^{-1}) are the water diffusivities at the boundary water content and the current micropore water content respectively and S_{ma} (m^3 m^{-3}) is the effective saturation in macropores given by (4):

$$S_{ma} = \frac{\theta_{ma}}{\theta_s - \theta_b} \tag{4}$$

where θ_s (m^3 m^{-3}) and θ_{ma} (m^3 m^{-3}) are the saturated water content and the macropore water content respectively. Using the Mualem/Brooks-Corey model for soil hydraulic properties, $D_{\theta mi}$ is given by (5):

$$D_{\theta mi} = \frac{K_b \Psi_b S_{mi}^{n+1/\lambda+1}}{\lambda\left(\theta_b - \theta_r\right)} \tag{5}$$

where Ψ_b (m) is the pressure head at the boundary between micro- and macropores, n (-) and λ (-) are the tortuosity factor and the pore size distribution index respectively, θ_r (m^3 m^{-3}) is the residual water content and S_{mi} is the effective saturation in micropores given by (6):

$$S_{mi} = \frac{\theta_{mi} - \theta_r}{\theta_b - \theta_r} \tag{6}$$

If the micropores become over-saturated (i.e. $\theta_{mi} > \theta_b$), any excess water is routed instantaneously into the macropores.

The MACRO model was calibrated for the first run using TDR measurements at three and two depths for site 1 and 2 respectively. The validation of the model was made with TDR measurements for the remaining two runs. The calibration procedure used a grid-search technique (see for instance Duan et al., 1992). The optimal parameter combination is identified by the minimum of the root mean square error under two constraints: the slope of the regression between predicted and measured values should be in the range of 0.9 to 1.1 and the coefficient of residual mass in the range of 0.001 to –0.001. The calibration was carried out using a software program designed to calibrate the MACRO model (Acutis et al., 2001), enabling the automatic execution of the model for each point of the chosen grid and an evaluation of several objective functions under user-defined constraints. In accordance with Loague and Green (1991), the coefficient of residual mass (CRM) is defined as:

$$CRM = \frac{\sum_{i=1}^{n} M_i - \sum_{i=1}^{n} E_i}{\sum_{i=1}^{n} M_i} \tag{7}$$

where M_i represents the measured values, E_i represents the estimated values and n is the number of observations.

The measured parameters used in the modelling included saturated water content, saturated hydraulic conductivity, initial water content and bulk density. The calibrated parameters comprised n^*, reflecting pore size distribution and tortuosity in the macropore system, and the minimum values defining the soil macropores (boundary water content, boundary hydraulic conductivity and boundary matrix potential). The MACRO model helped to define the boundary between the two flow domains. In the simulation, the evapotranspiration was set to zero, since MACRO model was run to simulate very short events neglecting the effect of the evapotranspiration. In addition to the validation of the model against measured TDR, we verified the outcome of the simulations with 2D image analysis of the resultant blue patches.

2.4. Dye Infiltration Experiment

A dye infiltration experiment was carried out in site 1 in order to verify the 1D (vertical) information obtained by the MACRO model and to visualise the heterogeneity of the tracer distribution pathways. Accordingly, 120 L of dye tracer solution were prepared by diluting 480 grams of Brilliant Blue FCF powder, also known as food-dye E133, in ordinary tap water (concentration = 4 g L^{-1}). On 23rd August 2005, 110 L of the prepared solution were applied in site 1 at a constant rate of 47.5 mm h^{-1} using a rainfall simulator. One day after this irrigation, a soil pit was excavated and vertical profiles were prepared at 0.20 m increments. A 0.1 x 0.1 m grid, made of a metal frame of 0.7 m x 1.0 m and rubber strings, was placed onto the soil profile, and the blue dye pattern was photographed with a digital camera (hp photosmart 945; resolution: 5 megapixels). The pictures were taken by daylight under a light tent to diffuse the light and to avoid direct radiation. The digitised 1.0 x 0.7 m cross-section grid contained 70 squares. The digital images obtained, that had a resolution of approximately 2,000 x 2,000 pixels, then underwent further processing.

2.5. Image Analysis and Optical Calibration

The final coverage of the stained areas was subsequently determined from profile images processed using the Photoshop CS2® software according to Alaoui and Goetz (2008) and briefly described here. The saturation of the blue stains was maximized to obtain three colours (yellow, green and blue) and two tinges (light and dark blue). The brown colour was then removed of the unstained areas. After that, the number of colours allowed was reduced so that only the four BB-related tints remained in the image. These colours were separated by cropping them successively and then pasting them into individual JPG files. By converting these pictures into grayscale images and performing tone value corrections, the tainted areas turned black, while the rest stayed white. The resulting patterns were then cut into 30 to 35 horizontal strips. The final steps were to distribute the black colour evenly across the surface of the corresponding strip and to note the resulting grayscale.

For a quantitative determination of different BB concentrations, a calibration that linked specific colours with corresponding BB concentration ranges were carried out. For this purpose, 10 standard solutions were prepared (BB concentration: 0.1, 0.5, 1, 2, 4, 6, 20, 40, 80 und 150 g L^{-1}) and the soil samples were saturated therein for five to six days. These were then photographed with the same camera as used before, under the same conditions as in the field.

3. Results

The results of the dye tracer experiment were only used to verify predicted WER since diffusion exchange, which is also important for solutes, is not taken into account by WER.

3.1. Modelling of Water Content

Once calibrated for the first run, the model also predicted reasonably well the two following runs using same parameter set (Figure 2). The best simulations were obtained under non-equilibrium conditions in both sites, which could be visually confirmed in the field (existence of macropores). While the effective diffusion path length *d* of the calibration varied between 1 and 30 mm, values of 18 mm at soil surface and 17 mm below in site 1 and of 20 mm throughout the soil profile in site 2 yielded the best simulation results (Table 2).

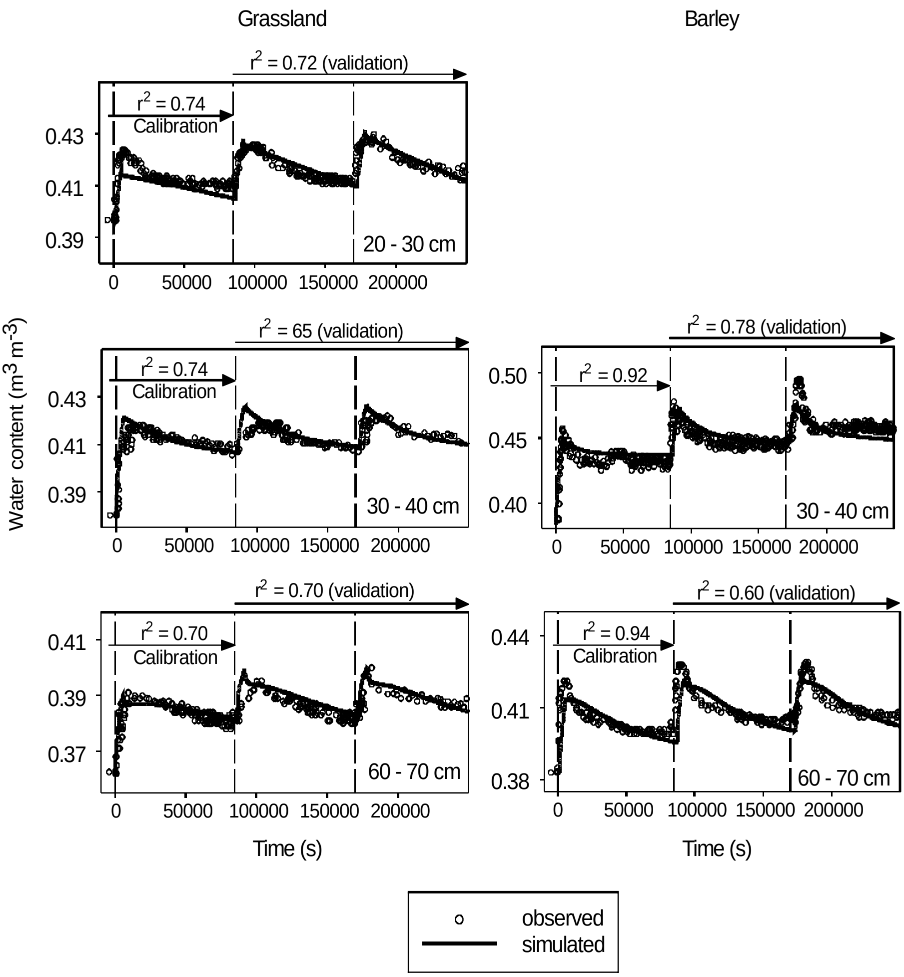

Figure 2. Calibration of MACRO model using in situ TDR measurements for grassland (site 1) and barley (site 2).

Table 2. Model input parameters: soil hydraulic properties at site 1 (grassland) and 2 (growing barley)

depth (m)	parameters								
	θ_s† (m^3 m^{-3})	θ_b‡ (m^3 m^{-3})	θ_r‡ (m^3 m^{-3})	ψ_b‡ (m)	λ ‡ (-)	K_s† (mm h^{-1})	K_b‡ (mm h^{-1})	d ‡ (mm)	n^* ‡ (-)
Site 1									
0-0.20	0.47	0.42	0	0.15	0.18	200	0.04	18	4
0.20-0.30	0.47	0.41	0	0.15	0.18	200	0.04	18	4
0.30-0.50	0.47	0.40	0	0.15	0.18	210	0.04	17	4
0.50-0.60	0.46	0.39	0	0.20	0.15	220	0.01	17	4
0.60-0.70	0.46	0.38	0	0.20	0.15	220	0.01	17	4
Site 2									
0-0.20	0.49	0.40	0	0.22	0.18	200	0.01	20	2
0.20-0.30	0.49	0.40	0	0.22	0.18	200	0.01	20	2
0.30-0.50	0.49	0.40	0	0.18	0.18	210	0.01	20	4
0.50-0.60	0.45	0.40	0	0.18	0.20	220	0.01	20	4
0.60-0.70	0.435	0.40	0	0.18	0.20	220	0.01	20	4

† Measured parameters.

‡ Parameters derived by calibration.

θ_s: saturated water content; θ_b: boundary water content; θ_r: residual water content; ψ_b: boundary tension;

λ: pore size distribution index; K_s: saturated hydraulic conductivity; K_b: boundary hydraulic conductivity; d: effective diffusion path length; and n^*: reflects pore size distribution index and tortuosity in the macropore system.

Figure 3 shows the very low WER from macropores to micropores, taking the input intensity (30 mm h^{-1}) into account. This demonstrates the efficient macropore flow through the silty clay texture. Due to the small matrix conductivities of such fine textures, the linings of macropores severely limit mass exchange (Köhne et al., 2002; Gerke and Köhne, 2002). Limited lateral mass exchange between macro- and micropores was observed in this study and is clearly visible in a photograph of a transversal section from 0.30 m depth (Figure 4). The average glaze of penetration did not exceed 4.5 mm for macropores with a mean diameter of 6 mm. It was also observed that between 0.30 and 0.40 m depth, the value of WER is relatively higher during the first irrigation and notably decreases between 0.60 and 0.70 m (Figure 3). The small values of WER reflecting stronger macropore flow may be linked with the high clay contents, varying from 43 % in topsoil to 52 % in subsoil (Table 1).

In fact, the degree of lateral water and solute mixing could be linked to morphological features of soil horizons (Vanderborht et al., 2001). Vervoort et al. (1999) demonstrated that a strongly developed soil structure promoted by large clay contents produced larger effective dispersivities, smaller mobile water contents and weaker lateral mass exchange. In sandy soils, lateral mixing is controlled by horizons of different textures.

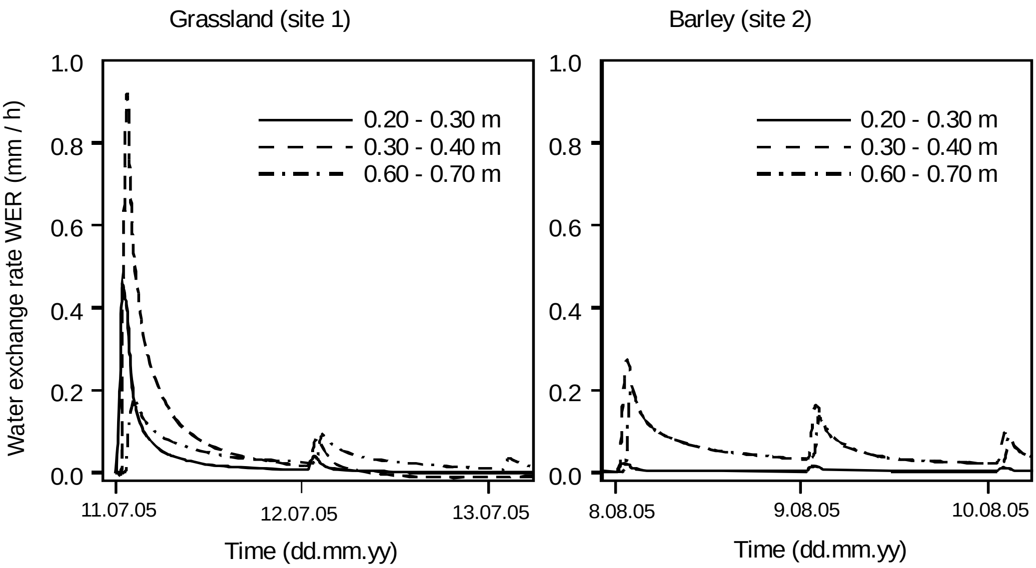

Figure 3. Predicted water exchange rate WER (positive from macropores to micropores) by the MACRO model in the silt clay material of Oensingen in site 1 (grassland) and 2 (growing barley).

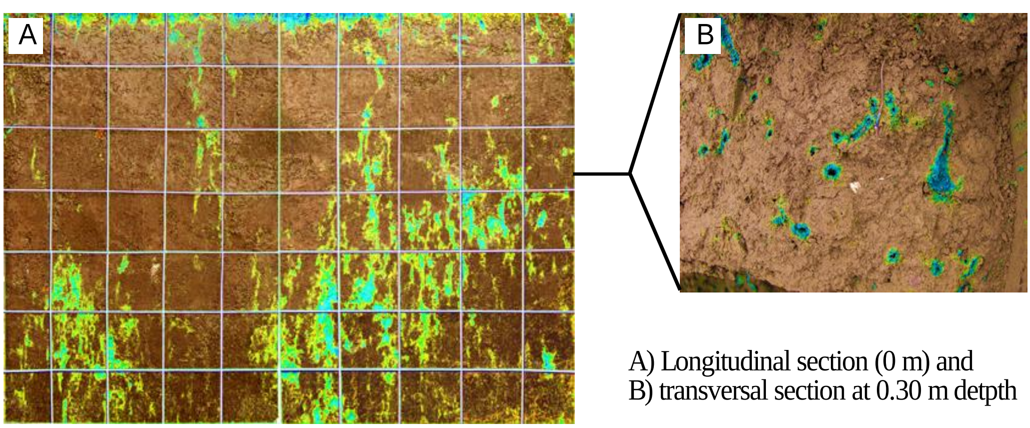

Figure 4. Longitudinal and transversal sections resulted from the image analysis of dye tracer in site 1.

WER was low at all depths in spite of the decrease of initial soil moisture from topsoil to subsoil in both sites (site 1: 0.40 $m^3\ m^{-3}$ between 0.20 and 0.30 m, 0.38 $m^3\ m^{-3}$ between 0.30 and 0.40 m, and 0.36 $m^3\ m^{-3}$ between 0.60 and 0.70 m; site 2: 0.35 $m^3\ m^{-3}$ between 0.30 and 0.40 m and 0.38 $m^3\ m^{-3}$ between 0.60 and 0.70 m for the first irrigation) (Table 3). This was likely due to water repellency effects that result from the generation of unstable flow, or ‘fingering’, leading to incomplete wetting of the soil matrix.

Figure 4 illustrates the restricted diffusion exchange between macropores and matrix in both transversal and longitudinal sections. A dye tracer experiment to visually verify the simulation results was only carried out in site 1 (grassland). While comparison of the two sites would have benefited from an identical infiltration experiment in the barley site, the dye tracer experiment nevertheless emphasises the compaction effect in enhancing macropore flow.

The BB surface density of the profiles from sections 0 m and 0.20 m was clearly weak between 0.10 and 0.30 m depth, indicating a restricted lateral mass exchange for this particular layer and consequently stronger macropore flow (Figure 3 and 4). Thus, the few macropores included conducted the applied solution efficiently. Below this layer an increase of surface density occurred. A plausible explanation for this particular stain pattern is that, below 0.30 m depth, a denser network of macropores with decreasing diameters leads to a greater lateral spread, thereby promoting the flow transfer from the more tortuous macropores to the matrix. This was confirmed by WER values, which were always higher below 0.30 m depth (0.91 mm h^{-1}) than above (0.46 mm h^{-1}) (site 1, Figure 3). These results were most likely due to the compaction effect on the soil surface; the bulk density was 1.66 g cm^{-3} between sections 0 m and 0.1 m and 1.55 g cm^{-3} between sections 0.1 m and 0.3 m. Our results are in agreement with the results obtained by Alaoui and Helbling (2006) in a loamy soil, which showed a weak lateral exchange from macropores to micropores in the topsoil due to the compacted matrix, while more extensive interaction was observed in the subsoil, indicating no effect of soil compaction at this horizon.

Alaoui and Goetz (2008) showed that the largest area of the high BB concentrations (0.5–4 g L^{-1}) was always found between 0.50 and 0.45 m depth. The corresponding minimum (smallest area of high BB concentrations in the range of 0.5–4 g L-1) was usually found at the bottom of the soil profiles. Even though the amount of clay increased with increasing depth, the tracer in soil near the field track penetrated deeper into the soil matrix, thus indicating a different ratio between the first three BB concentration ranges. This suggests that the solution moved through the macropores that were more tortuous with increasing depth, and thus was able to moisten a larger part of the matrix (Figure 4A). Diffusion related to depth was not clearly reflected by the effective diffusion path length *d* throughout the soil profile of site 1 (Table 2). In fact, it appears that the MACRO model is not sensitive to small variations of *d* (Alaoui et al., 2003). Accordingly, WER is a first order control in evaluating the degree of preferential flow. In order to improve the comparison between the two sites, it would be necessary to accomplish an identical dye infiltration experiment at the barley site.

3.2. Comparison of the Two Sites

The saturated hydraulic conductivities K_s of two sites were compared with each other. Site 1 was used as grassland and the site 2 as barley. By executing a couple of t-tests (α = 5%), it became obvious that the respective top- and subsoil K_s-values did not differ significantly out of a statistic point of view.

The average topsoil-porosity (0–0.50 m) of the grassland site was 0.47 m^3 m^{-3}, while the barley site had an average of 0.49 m^3 m^{-3}. By applying a statistic t-test, one can say that the difference is significant. The subsoil-porosity (0.60–0.70 m) of the grassland soil was 0.46 m^3 m^{-3}, whereas the corresponding barley-porosity was 0.44 m^3 m^{-3}; the difference here is significant too. In contrast, no significant difference was observed at depth of 0.50–0.60 m. Because of these obtained results, it is possible to conclude that tillage has a loosening effect on the topsoil at least to a depth of 0.30 m. This fact was also confirmed by the θ_s values and the pore volume distribution. The measured θ_s for site 1 was 0.47 $m^3 m^{-3}$ between 0 and 0.50 m and 0.46 $m^3 m^{-3}$ below that depth (Table 2). In comparison, θ_s of site 2 was higher between 0 and 0.50 m (0.49 $m^3 m^{-3}$) and smaller below (0.44–0.45 $m^3 m^{-3}$). Between 0.50 and 0.60 m there was no great difference amongst θ_s of the two sites, compared to site 1 (0.46 $m^3 m^{-3}$) it decreased below 0.60 m in site 2 (0.435 $m^3 m^{-3}$). Regarding the pore volume distribution of the topsoil, there was no significant difference among the pores of smaller radius (< 50 µm). The only significant difference, concerns pores with a diameter larger than 50 µm (Table 4). The subsoil pore volume distributions between the two sites were significantly different for all pore sizes. The subsoil of the grassland site had more pores with a diameter smaller than 3.2 µm; all the other ones were more frequent at the barley site.

In addition to other irrigation characteristics, Table 3 shows the magnitude of the decrease of water content within 24 hours during drainage process $\Delta\theta_2$. The observations related to the analysis of hydrodynamic water content variation during irrigations can be explained as follows:

1) The decrease of water content during drainage process $\Delta\theta_2$ was the highest between 0.2 and 0.3 m in site 1 in comparison with subsoil of same site (Table 3). This fact can be attributed to the rapid draining of macropores (e.g., Thomas and Phillips, 1979; Alaoui et al., 2003).

2) Considering the layer between 0.3 and 0.4 m, $\Delta\theta_2$ was higher in site 2 than in site 1 showing more pronounced drainage in site 2 confirming the observations related to the pore volume distribution and dye tracer experiment (Table 3).

Maximum water content θ_{max} measured at site 2 was the highest in comparison with the values measured at site 1. These observations are in agreement with the values of θ_s measured between 0 and 0.50 m depth for both sites (Table 2). Compared to the high input intensity (30 mm h^{-1}), predicted values of WER reflect the importance of macropore flow. The difference between the two sites is particularly large at a depth of 0.30–0.40 m (WER site 1 = 0.92 mm h^{-1}, WER site 2 = 0.27 mm h^{-1}). This may be related to the larger number of pores with diameters smaller than 32 µm in site 1 (Alaoui and Goetz, 2008). WER at a depth of 0.20–0.30 m showed no large difference either between the three irrigations or between the two sites. The fitted n^* was 4 throughout the soil profile of site 1; in site 2, it was 2 between 0 and 0.30 m depth, and 4 below 0.30 m depth. This MACRO parameter, which is applied only to the macropore area, reflects the high efficiency of macropore flow between 0 and 0.30 m depth in the barley site compared with the grassland site. It appears that the soil matrix in the barley site only starts to play a moderate role below 0.30 m depth.

Table 3. Characteristics of infiltration experiments conducted on sites 1 and 2

Site 1					
	Depth: 0.20–0.30 m				
Irrigation	θ_{init}	θ_{max}	θ_{end}	$\Delta\theta_1$	$\Delta\theta_2$
I	0.397	0.424	0.410	0.027	0.014
II	0.410	0.426	0.413	0.016	0.013
III	0.413	0.428	0.414	0.015	0.014
	Depth: 0.30–0.40 m				
Irrigation	θ_{init}	θ_{max}	θ_{end}	$\Delta\theta_1$	$\Delta\theta_2$
I	0.380	0.420	0.407	0.040	0.013
II	0.407	0.419	0.409	0.012	0.009
III	0.410	0.422	0.411	0.012	0.010
	Depth: 0.60–0.70 m				
Irrigation	θ_{init}	θ_{max}	θ_{end}	$\Delta\theta_1$	$\Delta\theta_2$
I	0.363	0.390	0.381	0.027	0.009
II	0.381	0.394	0.383	0.013	0.011
III	0.383	0.399	0.387	0.016	0.012
Site 2					
	Depth: 0.30–0.40 m				
Irrigation	θ_{init}	θ_{max}	θ_{end}	$\Delta\theta_1$	$\Delta\theta_2$
I	0.350	0.460	0.430	0.110	0.030
II	0.430	0.480	0.440	0.050	0.040
III	0.440	0.490	0.460	0.050	0.030
	Depth: 0.60–0.70 m				
Irrigation	θ_{init}	θ_{max}	θ_{end}	$\Delta\theta_1$	$\Delta\theta_2$
I	0.380	0.420	0.400	0.040	0.020
II	0.400	0.430	0.410	0.030	0.020
III	0.410	0.430	0.410	0.020	0.020

θ_{init}: water content prior to infiltration ($m^3\ m^{-3}$);
θ_{max}: maximum water content measured during infiltration ($m^3\ m^{-3}$);
θ_{end}: lower water content measured within 24 hours during drainage process ($m^3\ m^{-3}$);
$\Delta\theta_1$: increase of water content at the beginning of irrigation ($\theta_{max} - \theta_{init}$) ($m^3\ m^{-3}$);
$\Delta\theta_2$: decrease of water content during the drainage stage ($\theta_{max} - \theta_{end}$) ($m^3\ m^{-3}$).

Table 4. Comparison of the topsoil and subsoil pore volume distributions of the two sites

Topsoil	Diameter			
	< 3.2 µm	32–3.2 µm	50–32 µm	> 50 µm
Grassland [%]	85.0	8.0	1.0	6.0
Barley soil [%]	84.0	5.0	1.0	10.0
Subsoil	Diameter			
	< 3.2 µm	32–3.2 µm	50–32 µm	> 50 µm
Grassland [%]	92.1	3.7	0.2	4.0
Barley soil [%]	84.0	6.0	2.0	8.0

CONCLUSIONS

1. The interaction between matrix and macropores based on transversal section analysis and simulated water exchange rate (WER) is of great interest in evaluating the

importance of macropore flow. It was shown that macropore flow is negatively correlated to WER.

2. 2D image analysis of the blue patches confirmed the hydrodynamic aspects identified by 1D dual-porosity modeling providing useful insight on the difference between the barley and the grassland soils.
3. Barley has a notable effect on soil structure. In fact, in barley site, there was a higher pore volume with a diameter larger than 50 μm compared to grassland soil for same soil horizons. While, in the topsoil, the loosening effect may be due to the tillage, in the subsoil, this fact maybe attributed to the root system of the barley. The loosening effect of tillage in the topsoil of the barley site revealed in the laboratory analysis is confirmed by the results of MACRO simulations (small values of n^*, reflecting pore size distribution and tortuosity and WER).
4. The fact that the highest concentration values of the dye tracer are found at depth between 0.20 and 0.30 m in grassland, together with the lowest values of simulated WER, shows that the more tortuous macropores have been destroyed by compaction. Consequently, only the larger, less tortuous macropores remain and are efficient.

REFERENCES

Acutis, M., Mdaghri-Alaoui, A., Jarvis, N., Donatelli, M., 2001. A software for sensitivity analysis, calibration and inversion of MACRO model. Proceedings of the II international symposium "*Modelling Cropping System*" Firenze 16–17 July 2001, Florence, Italy, pp. 207–208.

Alaoui, A., Germann, P., Jarvis, N., Acutis, M., 2003. Dual-porosity and kinematic wave approaches to assess the degree of preferential flow in an unsaturated soil. *Hydrol. Sci. J*. 48(3), 455–472.

Alaoui, A., Helbling, A., 2006. Evaluation of soil compaction using hydrodynamic water content variation: Comparison between compacted and non compacted soil. *Geoderma* 134, 97–108.

Alaoui, A., Goetz, B., 2008. Dye tracer and infiltration experiments to investigate macropore flow. *Geoderma* 144, 279–286.

Booltink, H.W.G., Hatano, R., Bouma, J., 1993. Measurements and simulation of bypass flow in a structured clay soil. *J. Hydrol.* 148, 149–168.

Bronswijk, J.J.B., Hamminga, W., Oostindie, K., 1995. Field-scale solute transport in a heavy clay soil. *Water Resour. Res.* 31(3), 517–526.

Duan, Q., Gupta, V.K., Sorooshian, S., 1992. Effective and efficient global optimization for conceptual rainfall-runoff models. *Water Resour. Res*. 28(4), 1015–1031.

Faeh, A.O., Scherrer, S., Naef, F., 1997. A combined field and numerical approach to investigate flow processes in natural macroporous soils under extreme precipitation. *Hydrol. Earth Sys. Sci*. 1, 787–800.

Flühler, H., Durner, W., Flury, M., 1996. Lateral solute mixing processes—a key for understanding field-scale transport of water and solutes. *Geoderma* 70, 165–183.

Gerke, H.H., Köhne, J.M., 2002. Estimating Hydraulic Properties of Soil Aggregate Skins from Sorptivity and Water Retention. *Soil Sci. Soc. Am. J.* 66, 26–36.

Hendrickx, J.M.H., Flury, M., 2001. Uniform and preferential flow mechanisms in the vadose zone, in: Conceptual Models of Flow and Transport in the Fractured Vadose Zone. *Nat. Res. Council, Nat. Acad. Press*, Washington D.D., pp. 149–187.

Jarvis, N.J., 1994. The MACRO model Version 3.1 – Technical description and sample simulations. Reports and Dissertations no. 19, Department of Soil Science, Swedish University of Agricultural Sciences, Uppsala, Sweden, 51 pp.

Jarvis, N.J., 2007. A review of non-equilibrium water flow and solute transport in soil macropores: principles, controlling factors and consequences for water quality. *Eur. J. Soil Sci.* 58, 523–546.

Köhne, J.M., Gerke, H.H., Köhne, S., 2002. Effective Diffusion Coefficients of Soil Aggregates with Surface Skins. *Soil Sci. Soc. Am. J.* 66, 1430–1438.

Köhne, J.M., Köhne, S., Šimůnek, J., 2009a. A Review of Model Applications for Structured Soils: a) Water Flow and Tracer Transport, *J. Contam. Hydrol*. 104(1-4), 4–35.

Köhne, J.M., Köhne, S., Šimůnek, J., 2009b. A Review of Model Applications for Structured Soils: b) Pesticide Transport, *J. Contam. Hydrol*. 104(1-4), 36–60.

Kulli, B., Gysi, M., Flühler, H., 2003. Visualizing soil compaction based on flow pattern analysis. *Soil Till. Res*. 70, 29–40.

Loague, K, Green, R.E., 1991. Statistical and graphical methods for evaluating solute transport models: overview and application. *J. Contam. Hydrol*. 7, 51–73.

Logsdon, S.D., Nachabe, M.H., Ahuja, L.R., 1996. Macropore modeling: state of the science. Information Series No. 86, Water Resources Research Institute, Colorado State University, Fort Collins.

Othmer, H., Diekkrüger, B., Kutilek, M., 1991. Bimodal porosity and unsaturated hydraulic conductivity. *Soil Sci.* 152(39), 139–150.

Richards, L.A., 1931. Capillary conduction of liquids in porous mediums. *Physics* 1, 318–333.

Ritsema, C.J., Dekker, L.W., 1995. Distribution flow: A general process in the top layer of water repellent soils. *Water Resour. Res.* 31, 1187–1200.

Roth, K., Schulin, R., Flühler, H., Attinger, W., 1990. Calibration of Time Domain Reflectrometry for Water Content Measurement Using a Composite Dielectric Approach. *Water Resour. Res*. 26, 2267–2274.

Thomas, G.W., Phillips, R.E., 1979. Consequences of water movement in macropores. *J. Environ. Qual*. 8, 149–152.

Vanderborght, J., Vanclooster, M., Timmerman, A., Seuntjens, P., Mallants, D., Kim, D.-J. et al., 2001. Overview of inert tracer experiments in key Belgian soil types: relation between transport and soil morphological and hydraulic properties. *Water Resour. Res*. 37, 2873–2888.

Vervoort, R.W., Radcliffe, D.E., West, L.T., 1999. Soil structural development and preferential solute flow. *Water Resour. Res*. 35, 913–928.

Reviewed by

Jerzy Lipiec, Institute of Agrophysics, Polish Academy of Sciences, P.O. Box 201, 20-290 Lublin, Poland